

MESON PARTICLE-HOLE DYNAMICS ^a

E.E. KOLOMEITSEV and D.N. VOSKRESENSKY

*Gesellschaft für Schwerionenforschung, Planckstr. 1, 64291 Darmstadt
Moscow Engineering Physical Institute, Kashirskoe sh. 31, 115409 Moscow*

Particle-hole modes with quantum numbers of pions and negative kaons can propagate in nuclear matter. We discuss possible manifestations of these modes in experiments on heavy-ion collisions and on neutrino-nucleus scattering. Calculations of reaction rates in medium can be harmed by double counting, which arises because the very same quantum numbers can be carried in medium as by single particle excitations as by multi-particle ones. We argue that the optical theorem written in terms of the non-equilibrium Green's functions provides a convenient formalism (closed diagram technique) void of double counting.

1 Introduction

Going toward a consistent description of nuclear systems, one has to consider dynamics of strongly interacting particles in terms of in-medium dressed Green's functions which obey full or properly approximated Dyson's equations. In the present contribution we consider modifications of meson properties (pions and negative kaons) in nuclear matter due to the coupling to particle-hole excitations. This coupling induces virtual modes of meson propagation which can carry mesonic quantum numbers with energies smaller than the vacuum mode. Therefore, being easily excited they can manifest themselves in various experiments. We discuss production of particles in heavy-ion collisions (HIC) and scattering of anti-neutrino on nuclei. In this context we consider a double-counting problem arising in the calculation of the reaction rates in medium. This kind of problems can be avoided naturally within the closed diagram formalism based on the non-equilibrium Green's function technique of Schwinger-Kadanoff-Baym-Keldysh ^{1,2}. We illustrate this method by an example.

2 Meson Propagation in Nuclear Matter

Let us consider propagation of a meson M in isospin-symmetric nuclear matter with local density ρ and local temperature T . Speaking about "meson propagation" in medium, we mean propagation of in-medium excitation with mesonic

^aextended contribution to Proc. of Int. Workshop "Kadanoff-Baym Equations - Progress and Perspectives for Many-Body Physics" Rostock (Germany), September 20-24 1999, ed. M.Bonitz, World Scientific (2000)

quantum numbers. Properties of mesonic excitations are determined by in-medium retarded Green's function D_M^R , related to the free Green's function, D_M^{0R} via polarization operator Π_M^R as $D_M^R = [(D_M^{0R})^{-1} - \Pi_M^R]^{-1}$. All these quantities are functions of the meson frequency ω and momentum \mathbf{k} , and the polarization operator, containing complete information about meson interaction in medium, depends additionally on ρ and T .

For a strongly interacting system we cannot use the perturbation theory to select the most important processes contributing to the polarization operator. However, we can apply another approach suggested by Migdal within the theory of finite Fermi systems^{3,4}. In this approach, for any given interval of frequencies and momenta, one considers explicitly the graphs which strongly vary within this interval, whereas contributions of the graphs varying slowly are parameterized to fit available empirical data.

Utilizing this concept we decompose the retarded polarization operator of a meson M as follows

$$\Pi_M^R = \sum_a \text{graph}_1 + \text{graph}_2 + \sum_{M_a} \text{graph}_3. \quad (1)$$

Here the first graph takes explicitly into account the meson coupling to the baryon B_a -nucleon-hole states ($B_a N^{-1}$). This graph varies strongly for $\omega \sim m_{B_a} - m_N$, where m_{B_a} and m_N are corresponding baryon and nucleon masses. The sum goes over the baryon states allowed by the charge (strangeness for kaons) conservation. One usually is interested in a rather low-energy part of the meson spectrum, which is relevant at temperatures typical for a system under consideration, e.g., in HIC, $T \lesssim m_\pi$. Therefore only the lightest baryons should be included explicitly. The contribution of heavier baryons as well as the regular part of meson-baryon interaction are incorporated in the shaded block of the second diagram in (1). In the present consideration for the sake of simplicity we will treat baryons modified on the mean-field level only that corresponds to in-medium modification of a baryon mass. With this assumption we leave out a complicated problem of a self-consistent consideration of meson-baryon in-medium dynamics. The last issue can be addressed in the framework of a so-called Φ -derivable approach suggested by Baym⁵, see also Refs.^{6,7,8} and discussion below in sect. 6. The last term in (1) stands for the contribution of meson-meson interactions calculated with the full in-medium propagator of meson M_a . The meson self-interaction (case $M_a = M$) becomes extremely important and thereby should be explicitly treated at densities when mesonic modes become rather soft and a system is close to instability (condensation), or at large temperatures when the meson density is substantial. The

particular content of the hatched block in the last diagram is dependent on the approximation done for a baryon self-energy.

Being interested in the particle-hole mode propagation one also has to take into account modification of the meson-particle-hole vertex in medium, hatched vertex in the first diagram (1). This modification is given by

$$\begin{array}{c} B_a \\ \nearrow \\ N^{-1} \end{array} \begin{array}{c} \diagdown \\ \nearrow \\ N^{-1} \end{array} = \begin{array}{c} B_a \\ \nearrow \\ N^{-1} \end{array} \begin{array}{c} \diagdown \\ \nearrow \\ N^{-1} \end{array} + \sum_{B_b} \begin{array}{c} B_a \\ \nearrow \\ N^{-1} \end{array} \begin{array}{c} B_b \\ \diagdown \\ \diagup \\ N^{-1} \end{array} \begin{array}{c} \diagdown \\ \nearrow \\ N^{-1} \end{array}, \quad (2)$$

where the shaded block stands for an interaction irreducible with respect to $(B_a N^{-1})$ and one-meson states. For the small momenta and energies this interaction can be expressed through Landau-Migdal parameters³ of the short-range correlations. The outlined approach was utilized for pions in Refs. ^{4,9,10} and for kaons in Ref. ¹¹.

Pions in Medium. For pions the most important particle-hole contributions are the nucleon-nucleon-hole and the Δ -isobar-nucleon-hole in the first diagram (1) with $B_a = N, \Delta$. A regular part of the in-medium pion-nucleon interaction is extracted from phenomenological pion-nucleus optical potentials and low-energy theorems. The parameters of short-range NN interactions are adjusted to describe low-energy excitations in atomic nuclei. Information on the local interaction in $NN^{-1} \leftrightarrow \Delta N^{-1}$ and $\Delta N^{-1} \leftrightarrow \Delta N^{-1}$ channels is rather scarce and various parameterizations are in use^{3,4}.

To be specific we consider the isospin symmetrical nuclear matter at vanishing temperature. The resulting pion spectral density can be written approximately as a superposition of three quasiparticle (QP) branches $\omega_i(\mathbf{k})$ and a virtual nucleon-nucleon-hole mode below the line $\omega = k v_F$, where $v_F = p_F/m_N$ is the Fermi velocity,

$$A_\pi(\omega, \mathbf{k}) \approx \sum_{i=s,\pi,\Delta} 2\pi z_i(\mathbf{k}) \delta(\omega - \omega_i(\mathbf{k})) + \frac{2\beta k \omega}{\tilde{\omega}^4(\mathbf{k}) + \beta^2 \mathbf{k}^2 \omega^2} \theta(\omega < v_F k), \quad (3)$$

with $z_i(\mathbf{k}) = 1/[2\omega_i(\mathbf{k}) - \partial \text{Re} \Pi^R(\omega_i(\mathbf{k}), \mathbf{k})/\partial \omega]$. For normal nuclear matter density $\rho = \rho_0 = 0.17 \text{ fm}^{-3}$ one estimates $\beta \approx 0.7$. At $\rho > 0.5\rho_0$ and small ω the inverse pion propagator $D_\pi(0, \mathbf{k})^{-1} = -\tilde{\omega}^2(\mathbf{k}) = \mathbf{k}^2 + m_\pi^2 + \text{Re} \Pi_\pi^R(0, \mathbf{k})$ develops a roton-like minimum $\tilde{\omega}^2(\mathbf{k}) \approx \tilde{\omega}_c^2 + \gamma(\mathbf{k}^2 - k_0^2)^2/4k_0^2$ with some density dependent parameters $\gamma \sim 1$, $k_0 \sim p_F$ and $\tilde{\omega}_c < m_\pi$. The effective pion gap $\tilde{\omega}_c^2$ determines the degree of the pion-mode softening. At normal nuclear density, e.g., $\tilde{\omega}_c(\rho_0) \approx 0.8 m_\pi$.

Fig. 1 (left panel) shows pion spectrum calculated for $\rho = \rho_0$. Three QP branches are depicted by solid lines. The lowest branch ("s") is the spin-isospin sound induced by NN^{-1} correlations⁴. The modified pion branch

(“ π ”) goes below the vacuum pion branch because of attractive πNN and $\pi N\Delta$ interactions. The upper branch (“ Δ ”) corresponds to the propagation of the Δ -nucleon-holes states. The momentum dependent occupation factor $z_i(\mathbf{k})$ switches the strength of the spectral density from branch “ π ” at small momenta $k < 2m_\pi$ to branch “ Δ ” at large momenta $k > 3m_\pi$. The enhancement of the spectral density at low energy (contour plot in Fig. 1) is related to the population of the virtual pion mode $\omega = -i\tilde{\omega}^2(k)/\beta k$ (pole on the complex plane). These excitations are associated with a steady process of creation and annihilation of nucleon–nucleon-hole pairs. With increasing density the

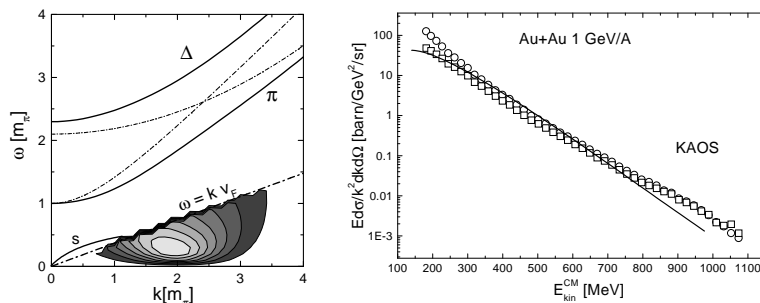


Figure 1: (Left panel) Pion spectrum in nuclear matter at saturation. Dash-dotted lines are the vacuum spectra of pions and Δ particles. Solid lines show the quasi-particle branches of pion excitations in medium. The contour plot depicts the spectral density of virtual pions. (Right panel) Invariant differential cross section of pion production in Au+Au collisions with energy 1 GeV per nucleon as a function of the pion kinetic energy in the center-of-mass system in comparison with experimental data¹² (squares stand for π^+ mesons and circles for π^-).

pion gap $\tilde{\omega}_c^2$ decreases and would be vanish at $\rho = \rho_c \sim (2 - 3) \rho_0$. At this density the system becomes unstable with respect to a pion condensation. In the vicinity of the critical point pion fluctuations increase dramatically and pion-pion interaction must be taken into account (the last diagram in (1)). The latter leads to that the pion gap $\tilde{\omega}_c^2$ makes a jump at ρ_c to a negative value and the nuclear system undergoes a first-order phase transition to a pion condensate state. We stress that in the context of a pion condensation, a special role is played: (i) by short-range NN^{-1} correlations, which reduce the strength of the particle-hole interaction preventing a pion condensation in nuclear matter at $\rho < \rho_0$, and (ii) by the in-medium $\pi - \pi$ interaction which prevents a second-order phase transition.

K⁻ in Medium. Applying Eq. (1) to kaons we have to consider the hyperon- and hyperon-resonance–nucleon-hole contributions, $B_a = \Lambda(1116)$,

$\Sigma(1190)$, and $\Sigma^*(1385)$. Since couplings of Σ and Σ^* particles to kaons and nucleons are much smaller than couplings of Λ , we consider here the (Λp^{-1}) contribution only. The parameters of the short-range Λp^{-1} interaction are estimated in Ref. ¹³. The regular part of the KN interaction (second term in (1)) is more elaborate. The K^-N interaction is inelastic already on the threshold due to the processes $K^-N \rightarrow \pi\Lambda(\Sigma)$. Therefore, one necessarily has to solve a coupled channel problem to develop a model for the K^-N interaction strength ¹⁴. Another peculiarity is that coupled channels generate the dynamical resonance $\Lambda^*(1405)$ just below the KN threshold ¹⁵. The pronounced resonance structure becomes broad at $\rho \gtrsim 0.2\rho_0$ and one can effectively describe the K^-N interaction in terms of mean-field potentials. For our estimation we utilize this potential picture ¹⁶ to describe regular part of the KN interaction. The net attractive potential acting on kaons is quite large (about 100 MeV for $\rho = \rho_0$). Also the interaction of kaons with in-medium pions is essential at finite temperatures in the case of strong pion softening ¹¹ ($\tilde{\omega}_c^2 \ll m_\pi^2$). Then the contribution of the last graph in Eq. (1) with $M_a = \pi$ is strongly attractive $\propto -T/\tilde{\omega}_c$.

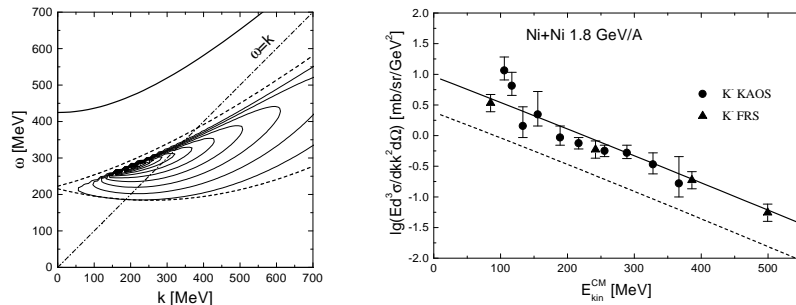


Figure 2: (Left panel) Spectral density of K^- excitations in nuclear matter at saturation. The upper curve shows the position of the quasiparticle kaon branch. Dashed curves border the (Λp^{-1}) continuum. Thin lines between them depict the ascending levels of kaon spectral density. (Right panel) Invariant differential cross section of K^- production in Ni+Ni collision with energy 1.8 GeV per nucleon as the function of the kaon kinetic energy in the center-of-mass system in comparison with experimental data ¹². Solid line depicts calculations with the in-medium spectral density, dashed line shows the results for the free kaon spectrum.

Fig. 2 (left panel) shows the resulting spectrum of negative kaons in nuclear matter at saturation. The solid line indicates the position of the quasi-particle branch determined by the mean-field potentials. The contour plot in the lower part (kaon spectral density) shows the distribution of kaon quantum numbers in the (Λp^{-1}) continuum. Note asymmetrical position of the maximum due to

short-range correlations. In further sections we will discuss how these modes could manifest themselves in experiments.

3 A Part of In-Medium Modes at Break up of Nuclear Fireball

In this section we consider possible manifestations of particle-hole excitations in experiments on HIC. In the course of HIC a dense and hot nuclear system (fireball) is formed. The system expands and cools down up to the moment when the inter-particle interaction ceases and the system disintegrates (breaks up). Particles which interact strongly with nuclear environment are confined inside the fireball until their mean free paths are shorter than the fireball size. Theoretical challenge is to calculate how in-medium excitations with given quantum numbers evolve to real on-shell particles at the breakup stage.

Assume that breakup happens within a time interval $t_0 - \frac{\tau_b}{2} < t < t_0 + \frac{\tau_b}{2}$, where τ_b is a typical *breakup time*. The momentum distribution of particles (bosons) after breakup (no interaction) is given by

$$\frac{dN^{\text{out}}}{dX^3 dk^3 / (2\pi)^3} = 2 \sqrt{m^2 + k^2} D_0^{-+} \left(t_0 + \frac{\tau_b}{2}, \mathbf{X}, t_0 + \frac{\tau_b}{2}, \mathbf{k} \right). \quad (4)$$

Here the Wigner transformation of a mesonic non-equilibrium Green's function, (in \pm notation of Ref. ²), is done in spatial coordinates only. The key point ¹⁷ is that if τ_b is sufficiently short then the Fock vector of state of the system does not change, i.e.,

$$D_0^{-+} \left(t_0 + \frac{\tau_b}{2}, \mathbf{X}, t_0 + \frac{\tau_b}{2}, \mathbf{k} \right) \approx D^{-+} \left(t_0 - \frac{\tau_b}{2}, \mathbf{X}, t_0 - \frac{\tau_b}{2}, \mathbf{k} \right), \quad (5)$$

where Green's function on l.h.s. corresponds to the vacuum and Green's function on r.h.s., to the interacting system (medium). Therefore we obtain

$$\frac{dN^{\text{out}}}{dX^3 dk^3 / (2\pi)^3} \approx 2 \sqrt{m^2 + k^2} \int_0^{+\infty} \frac{d\omega}{2\pi} D^{-+}(\omega, \mathbf{k}, \mathbf{X}, t_0). \quad (6)$$

Assuming now that strong interactions manage to keep nuclear system in local quasi-equilibrium up to its breakup stage we get

$$\frac{dN^{\text{out}}}{dX^3 dk^3} = 2 \sqrt{m^2 + k^2} \int_0^{\infty} \frac{d\omega}{(2\pi)^4} \frac{A(\omega, \mathbf{k}, \mathbf{X}, t_0; T(t_0, \mathbf{X}), \rho(t_0, \mathbf{X}))}{e^{\omega/T(t_0, \mathbf{X})} - 1}.$$

This expression relates the resulting particle yield to the in-medium spectral density, A , of excitations with given quantum numbers calculated at the breakup density $\rho(t_0, \mathbf{X})$ and the breakup temperature $T(t_0, \mathbf{X})$.

Eq. (5) is valid if the breakup lasts shorter than the time of the quantum-mechanical leap from an in-medium state (ω, \mathbf{k}) to a vacuum state $(\omega_k = \sqrt{m^2 + \mathbf{k}^2}, \mathbf{k})$, i.e. ^{9,10,17}, $\tau_b < 1/|\omega - \sqrt{m^2 + \mathbf{k}^2}|$. We would like to emphasize that the breakup model above is applicable only for those particles which path length is shorter than the fireball size right up to the breakup moment $t = t_0 - \tau_b/2$. Particles with the large path length compared to the fireball size have to be treated differently. Their yields are determined by the rates of direct reactions calculated within a closed-diagram formalism, see Sec. 6.

In our further consideration, we will use that pions with momenta $m_\pi < k < m_N$ and K^- mesons freeze out at the stage of the fireball breakup together with nucleons. This is supported by estimation of particle path lengths ^{18,19,20}. Estimation ⁹ of the breakup density and time in HIC gives $\rho_b \sim (0.5 - 0.7)\rho_0$, $\tau_b \sim 1/m_\pi$. At these conditions only the π and Δ branches can contribute to the total pion yield. If τ_b were shorter and also ρ_b were larger, the pion yield would be non-exponential $dN_\pi/dX^3 \sim k_0 \sqrt{m_\pi^2 + k_0^2} T / \sqrt{\gamma} \tilde{\omega}_c(\rho_b)$ for $\omega_c^2(\rho_b) \ll m_\pi^2$, due to a large contribution of nucleon-nucleon hole states. This would contradict to the available experimental data. Assuming simple spherical geometry of collision, we obtain the pion yield displayed on the right panel in Fig. 1, which shows a good agreement with experimental data for pion momenta $300 \text{ MeV} < k < 700 \text{ MeV}$.

Production of K^- mesons can be estimated in the same way as for pions. The only difference is that kaons have a finite negative chemical potential μ_K . Thresholds of reactions with strangeness production are high, therefore, the strange sub-system does not reach chemical saturation during the whole collision time. Knowing the experimental yield of K^+ mesons and taking into account the strangeness conservation in strong interactions we can estimate μ_K . Within the same model used for pions we obtain ²⁰ a satisfactory agreement with available experimental data if we utilize the in-medium spectral density. The results obtained with the free kaon spectrum underestimate the experiment by factor 2. This discrepancy emphasizes a role played by particle-hole modes in the K^- spectrum.

4 Electro-Weak Probe of Spectral Density

A direct probe of in-medium modification of particle properties would be the observation of some process which is forbidden for the particles with vacuum spectra. Sawyer suggested ^{21,22} to study reactions $\bar{\nu}_{e(\mu)} \rightarrow e^+(\mu^+) + \pi^-$ and $\bar{\nu}_{e(\mu)} \rightarrow e^+(\mu^+) + K^-$, the decays of an anti-neutrino in a nucleus into a positive lepton and an in-medium pion or kaon. Only the final lepton is detected experimentally whereas excitation with kaon or pion quantum numbers re-

mains inside the nucleus. To be specific we discuss below reaction with kaon production. The processes with pions were analyzed in Ref. ²²

The process $\bar{\nu}_{e(\mu)} \rightarrow e^+(\mu^+) + K^-$ can occur only if a kaon with space-like momentum can propagate in nuclear matter. The experimental observation of such a reaction would directly indicate that the kaon spectrum is modified in medium compared to its vacuum form. As we see from Fig. 2 (left panel) the Λ -proton-hole excitations can indeed carry kaonic quantum numbers with space-like momenta (region below the dash-dotted line). The differential cross section of this reaction on a nucleus with an atomic number A is equal to

$$\frac{d\sigma_l}{dE_l dx_l dt} = 2\pi r_0^3 A \left| \bar{\nu}_l \begin{array}{c} \nearrow l^+ \\ \blacklozenge \\ \leftarrow K^- \end{array} \right|^2 = r_0^3 A \frac{p_l}{8\pi E_\nu} A_K(\bar{\omega}_l, \bar{k}_l) V_K(E_\nu, \bar{\omega}_l, \bar{k}_l), \quad (7)$$

where we suggested that a nucleus is spherical and has constant density profile, and $r_0 \simeq 1.2$ fm. The quantity V_K is the effective vertex function shown by the fat diamond. We see that this process directly probes the kaon spectral density $A_K(\bar{\omega}_l, \bar{k}_l)$ at $\bar{\omega}_l = E_\nu - E_l$ and $\bar{k}_l = \sqrt{E_\nu^2 + p_l^2 - 2x_l E_\nu p_l}$. Here $E_{\nu(l)}$ and p_l are the neutrino (lepton) energy and momentum, respectively, and $x_l = \cos\theta_l$ is the neutrino-lepton scattering angle. The weak interaction of kaons changes in medium due to the kaon coupling to Λp^{-1} intermediate states, cf. Eqs. (15,16) below. Fig. 3 shows the differential cross section (7)

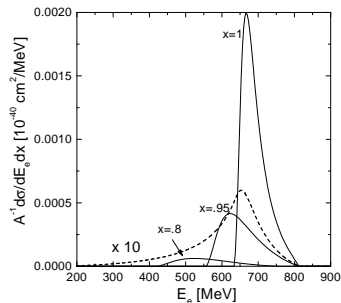


Figure 3: The differential cross section of positron production by antineutrinos with beam energy 1 GeV as a function of the lepton energy. Solid lines are calculated for three values of scattering angle. Dashed line shows the cross section integrated over the lepton angle.

for an anti-neutrino beam with energy 1 GeV ¹³. Obtained curves correspond to slices through the kaon spectral density.

5 Double Counting Problem

To estimate experimental feasibility of the in-medium kaon production by anti-neutrino one has to evaluate background processes. The background process to the kaon production by anti-neutrinos (7) is, e.g., the production of uncor-

related Λ particles

$$\begin{array}{c} \bar{\nu}_l \quad l^+ \\ \swarrow \quad \searrow \\ p \quad \blacksquare \quad \Lambda \end{array} + \begin{array}{c} \bar{\nu}_l \quad l^+ \\ \swarrow \quad \searrow \\ p \quad \bullet \quad \Lambda \end{array} \quad (8)$$

Here the fat square denotes an in-medium weak current $p \rightarrow \Lambda$ irreducible with respect to an one-kaon exchange and the fat circle takes into account baryon-baryon correlations. Thus, we are coming to the problem to calculate rates of the processes (7) and (8) in medium. Proceeding naively, one would sum up diagrams (8) with Λ and the diagram (7) with the kaon according to the standard technique for vacuum diagrams but with the in-medium corrected vertices and kaon propagator. This leads, however, to *double counting*. To demonstrate it explicitly we use the optical theorem and write the contributions of the kaon-production process (7) and, e.g., of the second process with Λ production in Eq. (8)

$$\sum_{\{K^-\}} |\mathcal{M}_{K^-}|^2 + \sum_{\{p, \Lambda\}} |\mathcal{M}_{\Lambda}^{II}|^2 = 2 \text{Im} \left(\begin{array}{c} l^+ \quad \bar{\nu}_l \quad l^+ \\ \swarrow \quad \searrow \quad \swarrow \quad \searrow \\ \bar{\nu}_l \quad \quad \quad \bar{\nu}_l \quad \quad \quad \Lambda \end{array} + \begin{array}{c} l^+ \quad \bar{\nu}_l \quad l^+ \\ \swarrow \quad \searrow \quad \swarrow \quad \searrow \\ \bar{\nu}_l \quad \quad \quad \bar{\nu}_l \quad \quad \quad \Lambda \end{array} \right) \quad (9)$$

We immediately observe that the self-energy insertion in the second diagram generates the doubled terms in perturbation series since the second diagram (6) contains effectively an additional self-energy insertion to the full Green's function of a kaon. This example shows that the standard Feynman diagram technique, based entirely on the asymptotic state concept, cannot be directly applied to the description of reactions in medium. Redrawing Feynman diagrams with full in-medium propagator and vertices leads to double counting. In the particular case discussed above, the problem with double counting arises because we have asked an incorrect question in the very beginning: What is the rate of in-medium kaon production in the scattering of anti-neutrinos on a nucleus? Since one does not detect in-medium particles, the states of in-medium K^- and Λ particles are mixed and not resolved and we actually deal with an inclusive experiment testing the reaction $\bar{\nu}_l + A \rightarrow l^+ + X$. Therefore the correct question, which only can be answered by such an experiment, is about the *total rate* of the reaction $\bar{\nu}_l + A \rightarrow l^+ + X$, where one should thoroughly count all possible X states.

6 Optical Theorem Formalism

A kind of problems illustrated above can be avoided using the closed-diagram technique^{23,24,13}. In this approach one directly addresses the question about a total rate of a process in terms of observable initial and final states.

In our example the total rate of lepton production by an anti-neutrino scattering on a nucleus is given by

$$\frac{d\mathcal{W}_{\bar{\nu} \rightarrow l^+}^{\text{tot}}}{dt} = \frac{d^3 p_l}{(2\pi)^3 4 E_\nu E_l} \sum_X \langle \bar{\nu}_l | S^+ | l^+ + X \rangle \langle l^+ + X | S | \bar{\nu}_l \rangle, \quad (10)$$

where X is the complete set of *all* possible states constrained only by energy-momentum conservation. $S \approx 1 - \int_0^\infty dx^0 T \{V_{\text{weak}}(x) S_{\text{nucl}}(x)\}$ is the scattering matrix, with V_{weak} related to the weak interaction vertex and S_{nucl} being S-matrix of the strong interaction. The crossing relation,

$$\sum_X \langle \bar{\nu}_l | S^+ | l^+ + X \rangle \langle l^+ + X | S | \bar{\nu}_l \rangle = \sum_X \underbrace{\langle \bar{\nu}_l + l^- | S^+ | X \rangle}_{-} \underbrace{\langle X | S | \bar{\nu}_l + l^- \rangle}_{+}, \quad (11)$$

invites to present the rate (10) by a *closed diagram*

$$\frac{d\mathcal{W}_{\bar{\nu} \rightarrow l^+}^{\text{tot}}}{dt} = \frac{d^3 p_l}{(2\pi)^3 4 E_\nu E_l} \times + \text{blob}^-, \quad (12)$$

where the \pm signs are placed according to the left-hand side of Eq. (11). The remaining task is to calculate the $(-+)$ blob in Eq. (12).

\pm **Notations.** The \pm notations are convenient since they indicate the positions of a cut of diagrams (through (\pm, \mp) -lines). According to this cut one can classify diagrams contributing to the blob in (12) with respect to the number of internal (\pm, \mp) -lines²³.

$$+ \text{blob}^- = + \text{blob}^+ + \text{blob}^- + \text{blob}^+ + \text{blob}^- + \dots$$

In many cases, e.g., in the quasiparticle and quasiclassical limits such a classification of the diagrams is very convenient. Indeed $G_{\text{F}}^{-+} = iA_{\text{F}} n_{\omega}^{\text{F}}$ and $G_{\text{F}}^{+-} = iA_{\text{F}}(1 - n_{\omega}^{\text{F}})$ and the pair of fermion Green's functions $G^{-+}G^{+-}$ is a very sensitive function of particle occupations in both small and large temperature limits. For instance, at low temperatures and in the quasiparticle limit for fermion Green's functions each $G^{-+}G^{+-}$ pair suppresses contribution of the diagram by a factor $\sim (T/\epsilon_{\text{F}})^2$, where ϵ_{F} is the Fermi energy.

Please notice that self-energy $(+, -)$ and $(-, +)$ insertions to the $(+, -)$ and $(-, +)$ Green's functions are permitted if one works in the framework of the quasiparticle approximation. In general case self-energy insertions to the Green's functions are not permitted²⁴ since they are included in full Green's

functions. Also beyond the quasiparticle approximation cutting of the diagrams has only a symbolic meaning, since integrations are done with the full spectral functions.

In general case any diagram with m (+, -)-lines and n (-, +)-lines can be opened as follows^{8,24}

$$\sum_{m,n} \sum_{\alpha,\beta} \left[\text{Diagram with } m \text{ (+, -) lines and } n \text{ (-, +) lines} \right] = \sum_{m,n} \sum_{\alpha,\beta} \int \prod_{i=1}^n \frac{d^4 p_i}{(2\pi)^4} A_i(p_i^0, \mathbf{p}_i) f_i(X, p_i) \times (2\pi)^4 \delta^{(4)} \left(\sum_{i=1}^n p_i - \sum_{j=1}^m p_j \right) V_\alpha V_\beta^* \prod_{j=1}^m \frac{d^4 p_j}{(2\pi)^4} A_j(p_j^0, \mathbf{p}_j) [1 \pm f_j(X, p_j)], \quad (13)$$

where A_i is the spectral density of particle i and f_i is its population factor. Matrix elements V_β^* and V_α contain no (\pm, \mp)-lines and can be calculated according to standard diagram rules. Separating all cuts explicitly and avoiding self-energy insertions in the closed diagrams with full Green's functions²⁴ we include properly modification of both particle propagation and interaction in medium, and naturally avoid the mentioned double counting problem.

Separation of Physical Sub-processes. Now we can come back to our original question about strangeness production by anti-neutrinos. The various contributions from $\{X\}$ in Eq. (10) can be classified according to global characteristics, such as strangeness, parity etc. Then, we can write

$$\frac{d\mathcal{W}_{\bar{\nu} \rightarrow l^+}^{\text{tot}}}{dt} = \frac{d^3 p_l}{(2\pi)^3 4 E_\nu E_l} \left(\begin{array}{c} l^+ \\ + \\ \bar{\nu}_l \end{array} \left[\Delta S=0 \right] \begin{array}{c} \bar{\nu}_l \\ - \\ l^+ \end{array} + \begin{array}{c} l^+ \\ + \\ \bar{\nu}_l \end{array} \left[\Delta S=-1 \right] \begin{array}{c} \bar{\nu}_l \\ - \\ l^+ \end{array} + \dots \right).$$

The first term represents all processes without strangeness transfer $\Delta S = 0$ in the intermediate states. The second term contains the processes with strangeness transfer $\Delta S = -1$. Ellipses symbolize all other processes. Each blob can be considered as a propagation of some quanta of the in-medium interaction with certain quantum numbers.

An Exercise. In this section we outline main steps for the calculation of kaon and Λ production by anti-neutrinos¹³ within the closed diagram technique.

Step I is to separate kaon and Λ -proton-hole states, as

$$\begin{array}{c} l^+ \\ + \\ \bar{\nu}_l \end{array} \left[\Delta S=-1 \right] \begin{array}{c} \bar{\nu}_l \\ - \\ l^+ \end{array} = \begin{array}{c} l^+ \\ + \\ \bar{\nu}_l \end{array} \dots \begin{array}{c} \bar{\nu}_l \\ - \\ l^+ \end{array} + \begin{array}{c} l^+ \\ + \\ \bar{\nu}_l \end{array} \left[K^- \right] \begin{array}{c} \bar{\nu}_l \\ - \\ l^+ \end{array} + \begin{array}{c} l^+ \\ + \\ \bar{\nu}_l \end{array} \left[\Lambda \right] \begin{array}{c} \bar{\nu}_l \\ - \\ l^+ \end{array} \dots \quad (14)$$

Ellipses stand for diagrams with more (\pm, \mp) lines, the contribution of which is suppressed by the smaller phase space. The dotted line indicates the kaon

corrected by the regular part of the polarization operator only.

Step II is to renormalize weak interaction vertices. The shaded block in (14) is irreducible with respect to (\pm, \mp) kaon and Λ -proton-hole lines. It can contain only the lines of one given sign, all $(--)$ or $(++)$. Dropping the sign notation we again separate explicitly the particle-hole contribution to the weak interaction vertex

$$\begin{array}{c}
 l^+ \quad \Lambda \quad l^+ \\
 \swarrow \quad \nearrow \quad \swarrow \quad \nearrow \quad \swarrow \quad \nearrow \\
 \text{shaded block} = \text{triangle} + \text{circle} \\
 \bar{\nu}_l \quad p \quad \bar{\nu}_l \quad p \quad \bar{\nu}_l \quad p
 \end{array} \quad (15)$$

with bare weak interaction, including the local $p \rightarrow \Lambda$ current and the interaction mediated by the kaon,

$$\begin{array}{c}
 l^+ \quad \Lambda \quad l^+ \quad \Lambda \quad l^+ \quad \Lambda \\
 \swarrow \quad \nearrow \quad \swarrow \quad \nearrow \quad \swarrow \quad \nearrow \\
 \text{triangle} = \text{kaon} + \text{square} \\
 \bar{\nu}_l \quad p \quad \bar{\nu}_l \quad p \quad \bar{\nu}_l \quad p
 \end{array} \quad (16)$$

Step III is to renormalize the Λp interaction. The shaded block in the last term in Eq. (15) denotes the full Λ -particle-proton-hole interaction, which obeys the following equation

$$\begin{array}{c}
 \Lambda \quad \Lambda \quad \Lambda \quad \Lambda \quad \Lambda \quad \Lambda \\
 \swarrow \quad \nearrow \quad \swarrow \quad \nearrow \quad \swarrow \quad \nearrow \quad \swarrow \quad \nearrow \\
 \text{shaded block} = \text{circle} + \text{loop} \\
 p \quad p \quad p \quad p \quad p \quad p
 \end{array} \quad (17)$$

with the bare Λ -proton-hole interaction

$$\begin{array}{c}
 \Lambda \quad \Lambda \quad \Lambda \quad \Lambda \quad \Lambda \quad \Lambda \\
 \swarrow \quad \nearrow \quad \swarrow \quad \nearrow \quad \swarrow \quad \nearrow \\
 \text{circle} = \text{kaon} + \text{square} \\
 p \quad p \quad p \quad p \quad p \quad p
 \end{array} \quad (18)$$

containing the kaon-exchange channel (the kaon includes the regular part of polarization operator (1) irreducible with respect to the particle-hole) as well as the (Λp^{-1}) short-range interaction. Please notice that, since, for the sake of simplicity, we have decided to treat baryon Green's functions as modified only by mean fields, there is no difference in procedure of diagram cutting for a quasiparticle case and for a general case.

Fig. 4 shows the positron production cross section in reaction $\bar{\nu}_e + A \rightarrow e^+ + X$ in strange sector, $\Delta S = -1$, i.e. in reactions $\bar{\nu}_e \rightarrow e^+ + K^-$ and $\bar{\nu}_e + p \rightarrow e^+ + \Lambda$. Differential cross section decreases with increasing positron scattering angle. The angular integrated cross section remains almost constant in a wide interval of the positron energy. Figs. 3 and 4 show that reaction $\bar{\nu}_e + p \rightarrow e^+ + \Lambda$ gives the main contribution to the strangeness production by anti-neutrinos on a nucleus. This process occurs in the same kinematic

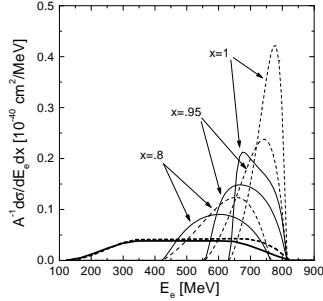


Figure 4: Differential cross section (per particle) of positrons produced in reactions $\bar{\nu}_e \rightarrow e^+ + K^-$, $\bar{\nu}_e + p \rightarrow e^+ + \Lambda$ by anti-neutrino of beam energy 1 GeV. Thin solid lines correspond to calculations with in-medium vertex renormalization whereas thin dashed lines, without inclusion of short-range ΛN correlations. Thick solid and dashed lines depict cross sections integrated over the lepton angle θ_l with and without vertex renormalization.

region as the reaction $\bar{\nu}_e \rightarrow e^+ + K^-$. Also we should stress that both strange ($\Delta S = -1$) and non-strange ($\Delta S = 0$) contributions to the angular integrated cross sections are found to be of the same order of magnitude. Nevertheless, being related to the distinct kinematic regions at the fixed neutrino-lepton scattering angle, they can be distinguished. They also can be distinguished with the help of a simultaneous identification of strange particles in the final state. To separate a very small contribution of the K^- channel shown in Fig. 3 one needs a much more peculiar analysis associated with detecting particles, in which in-medium kaon may decay.

7 Conclusion

We considered meson particle-hole propagation in nuclear matter. On the example of pions and negative kaons we showed how particle-hole modes modify the spectra of mesonic excitations. We argued that in-medium mesonic modes can manifest themselves in the particle yields measured in heavy-ion collisions at SIS energies. In particular we used a concept of breakup stage of HIC, during which in-medium excitations evolve to the real on-shell particles. The calculated pion and kaon yields are in agreement with experimental data if the in-medium mesonic spectra are utilized.

We discussed another method to probe the in-medium particle spectral density by the anti-neutrino-induced reactions. On this example we discussed a double counting problem, which arises in calculation of reaction rates in medium within standard Feynman-diagram technique. We presented closed diagram formalism based on the optical theorem, formulated in terms of non-equilibrium Green's functions. This technique allows to calculate the rates of processes involving as single-particle (meson) as multi-particle (particle-hole) modes without any double counting. It naturally incorporates also modification of inter-particle interactions in medium.

Acknowledgements. We are grateful to R. Dahl, H. van Hees, Yu.B. Ivanov, J. Knoll, and M. Lutz for discussions. We highly appreciate hospitality rendered to us at the GSI theory group. This work was supported in part by BMBF (WTZ project RUS-656-96). One of us (E.E.K) acknowledges partial support of DFG allowing him to participate at this workshop.

References

1. L.P. Kadanoff, G. Baym, *Quantum Statistical Mechanics* (Benjamin, 1962).
2. E.M. Lifshitz, L.P. Pitaevskii, *Physical Kinetics* (Pergamon Press, 1981).
3. A.B. Migdal, *Theory of Finite Fermi Systems and Properties of Atomic Nuclei* (Wiley and Sons, 1967).
4. A.B. Migdal et al., *Phys. Rep.* **192**, 179 (1990).
5. G. Baym, *Phys. Rev.* **127**, 1391 (1962).
6. W. Weinhold et al., *Phys. Lett.* **B433** 236 (1998).
7. Yu.B. Ivanov et al., *Nucl. Phys.* **A657**, 413 (1999); nucl-th/9905028.
8. Yu.B. Ivanov et al., this proceedings.
9. D.N. Voskresensky, *Sov. J. Nucl. Phys.* **50**, 983 (1989); *Nucl. Phys.* **A555**, 293 (1993).
10. D.N. Voskresensky et al., *Int. J. Mod. Phys.* **E4**, 1 (1995).
11. E.E. Kolomeitsev et al., *Nucl. Phys.* **A588**, 889 (1995).
12. pion: A. Wagner et al., *Phys. Lett.* **B420**, 20 (1998); kaon: R. Barth et al., *Phys. Rev. Lett.* **78**, 4007 (1997); A. Schröter et al., *Z. Phys.* **A350**, 101 (1994).
13. E.E. Kolomeitsev, D.N. Voskresensky, *Phys. Rev.* **C60**, 034610 (1999).
14. A.D. Martin, *Nucl. Phys.* **B179**, 33 (1981).
15. T. Waas et al. *Phys. Lett.* **B365**, 12 (1996); M. Lutz, *ibid* **B426**, 12 (1998).
16. G.E. Brown, *Nucl. Phys.* **A574**, 217c (1994); C.H. Lee, *ibid.* **A585**, 401 (1995).
17. A.V. Senatorov, D.N. Voskresensky, *Phys. Lett.* **B219**, 31 (1989).
18. D.N. Voskresensky, A.V. Senatorov, *Sov. J. Nucl. Phys.* **53**, 935 (1991).
19. D.N. Voskresensky, E.E. Kolomeitsev, *Phys. At. Nucl.* **56**, 252 (1993); *ibid* **58**, 126 (1995).
20. E.E. Kolomeitsev et al., *Int. J. Mod. Phys.* **E5**, 313 (1996).
21. R.F. Sawyer, A. Soni, *Phys. Rev. Lett* **38**, 1383 (1977); R.F. Sawyer, *Phys. Rev. Lett.* **73**, 3363 (1994).
22. N.G. Kelkar et al., *Phys. Rev.* **C55**, 1964 (1997); H. Kim et al, *ibid* **C51**, 2739 (1995).

23. D.N. Voskresensky, A.V. Senatorov, *Sov. J. Nucl. Phys.* **45**, 411 (1987).
24. J. Knoll, D.N. Voskresensky, *Phys. Lett.* **B351**, 43 (1995); *Ann. Phys. (N.Y.)* **249**, 532 (1996).